DOI: 10.1002/((please add manuscript number))

Article type: Full Paper

Efficient, Thermally Stable, and Mechanically Robust All-Polymer Solar Cells Consisting of the Same Benzodithiophene Unit-Based Polymer Acceptor and Donor with High Molecular Compatibility

Jin-Woo Lee,[⊥,†] Cheng Sun,[⊥,§] Boo Soo Ma,[‡] Hyeong Jun Kim,[†] Cheng Wang,[∥] Jong Min Ryu,[⊥] Chulhee Lim,[†] Taek-Soo Kim,[,‡] Yun-Hi Kim,[*,§] Soon-Ki Kwon,[*,⊥] and Bumjoon J. Kim[*,†]*

[†]J.-W. Lee, Dr. H. J. Kim, C. Lim, Prof. B. J. Kim

Department of Chemical and Biomolecular Engineering, Korea Advanced Institute of Science and Technology (KAIST), Daejeon 34141, Republic of Korea

E-mail: bumjoonkim@kaist.ac.kr

[§]C. Sun, Prof. Y.-H. Kim

Department of Chemistry and RIGET, Gyeongsang National University, Jinju 660-701, South Korea

E-mail: ykim@gnu.ac.kr

[#]B. S. Ma, Prof. T.-S. Kim

Department of Mechanical Engineering, Korea Advanced Institute of Science and Technology (KAIST), Daejeon 34141, Republic of Korea

E-mail: tskim1@kaist.ac.kr

[‖]Dr. C. Wang

Advanced Light Source, Lawrence Berkeley National Laboratory, 1 Cyclotron Road, Berkeley, CA 94720, United States

[‡]J. M. Ryu, Prof. S.-K. Kwon

Department of Materials Engineering and Convergence Technology and ERI, Gyeongsang National University and ERI, Jinju, 660-701, Korea

E-mail: skwon@gnu.ac.kr

Keywords: all-polymer solar cells; BDT-based polymer acceptor; mechanical robustness; stretchability; molecular compatibility

Abstract

All polymer solar cells (all-PSCs) are a highly attractive class of photovoltaics for wearable and portable electronics due to their excellent morphological and mechanical stabilities. Recently, new types of polymer acceptors (P_As) consisting of non-fullerene small molecule acceptors (NFSMAs) with strong light absorption have been proposed to enhance the power conversion efficiency (PCE) of all-PSCs. However, polymerization of NFSMAs often reduces entropy of mixing in PSC blends and prevents the formation of intermixed blend domains required for efficient charge generation and morphological stability. One approach to increase compatibility in these systems is to design P_As that contain the same building blocks as their polymer donor (P_D) counterparts. Here we report a series of NFSMA-based P_As [P(BDT2BOY5-X), (X = H, F, Cl)], by copolymerizing NFSMA (Y5-2BO) with benzodithiophene (BDT), a common donating unit in high performance P_Ds such as PBDB-T. All-PSC blends composed of PBDB-T P_D and P(BDT2BOY5-X) P_A show enhanced molecular compatibility, resulting in excellent morphological and electronic properties. Specifically, PBDB-T:P(BDT2BOY5-Cl) all-PSC has a PCE of 11.12%, which is significantly higher than previous PBDB-T:Y5-2BO (7.02%) and PBDB-T:P(NDI2OD-T2) (6.00%) PSCs. Additionally, the increased compatibility of these all-PSCs greatly improved their thermal stability and mechanical robustness. For example, the crack onset strain (COS) and toughness of the PBDB-T:P(BDT2BOY5-Cl) blend were 15.9% and 3.24 MJ m^{-3} respectively, in comparison to the PBDB-T:Y5-2BO blends at 2.21% and 0.32 MJ m^{-3}.

1. Introduction

Polymer solar cells (PSCs) are highly attractive as next-generation wearable power generators due to their light-weight, low cost, and stretchability.[1] One remarkable advancement for PSCs is achieved by the use of non-fullerene small molecule acceptors (NFSMAs),[2] significantly increasing power conversion efficiencies (PCEs) of single junction devices. Compared to conventional fullerene-based acceptors, NFSMAs based on highly fused backbones with strong dyes have much higher light absorption and tunable energy levels.[2a, 2b, 2e, 3] Despite these developments, the long-term stability of NFSMA based PSCs remains a major challenge in the field.[4] Moreover, the mechanical properties and stretchability of these PSCs do not meet the requirements of practical portable and wearable power generators.[5] These drawbacks stem from the strong crystallinities and high diffusion properties of NFSMAs, resulting in sharp domain interfaces and poor morphological stabilities in their PSC blends.[4, 6]

All-polymer solar cells (all-PSCs), consisting of a polymer donor (P_D) and a polymer acceptor (P_A), are known for their superior mechanical and morphological stabilities against thermal annealing, light exposure, and donor/acceptor compositional deviations.[4,

7] However, the PCEs of all-PSCs reported to date are far behind those of NFSMA-based PSCs (17-18%).[7b, 7r, 7t, 7u] Additionally, most of the P_As are based on perylene diimide (PDI) or naphthalene diimide (NDI) derivatives that have low absorption coefficients (~ 0.3 – 0.4 × 10^5 cm^{-1}) and charge mobilities (~ 10^{-5} $cm^2V^{-1}s^{-1}$),[7r, 7t, 7u, 8] limiting the short-circuit current density (J_{sc}) and overall PCE of their all-PSCs.[7r, 7t]

To address these issues, new types of P_As with excellent light absorption and charge carrier mobilities have been developed by polymerizing NFSMA moieties.[4a, 6, 7b, 7g, 9] For instance, Yao et al. used IDTIC NFSMA building blocks to form PFBDT-IDTIC P_As and developed all-PSCs with a PCE of 10.4%.[7b] More recently, Wang et al. reported all-PSCs with a PCE of 13.4 % using a Y5 based NFSMA P_A and a single thiophene donating unit.[7g] While all-PSCs with reasonably high PCEs have been demonstrated using NFSMA-based P_As, the strong self-aggregation behaviors of the P_As and the reduced entropy of mixing in the polymer blends compared with that in the NFSMA-based blends often causes severe phase separations of the all-PSC blends. Thus, control of the solution preparation and processing conditions by considering the pre-aggregation properties of both the P_Ds and P_As is crucial in optimizing the blend morphology.[10] In addition, the incompatibility between P_Ds and P_As leads to the formation of the interfaces with

reduced interfacial area and narrow interfacial width in their blends, typically decreasing charge generation, mechanical robustness and thermal stability in these all-PSCs.[7r] It is well known that the entropy of P_D-P_A mixing is inversely proportional to the degree of polymerization of the polymers.[7r, 11] Thus, at the high molecular weights, required to form chain entanglements that realize mechanical and morphological stabilities of all-PSCs,[4b, 7p, 12] the entropic contribution is very small and the miscibility of the system is mainly dependent on the enthalpy of mixing. As a result, the mechanical properties and the morphological stabilities of the all-PSCs with NFSMA-based P_As are not high. For example, their crack onset strains (COSs) are limited to lower than 10%.[4a] Therefore, a new material design strategy is needed to create highly efficient and mechanically robust NFSMA-based all-PSCs.

Here, we report a new family of NFSMA-based P_As by co-polymerizing Y5-2BO NFSMA with benzodithiophene (BDT) moieties, which are commonly used building blocks in many high-performance P_Ds. Our hypothesis is that the NFSMA-derivative P_As containing the same BDT units as their P_D counterparts should compensate for the lower entropy of mixing in their blends, enhancing the molecular compatibility of the system and improving the mechanical, thermal and electronic properties of their all-PSCs. In

addition, fluorine (F) and chlorine (Cl) halogens are introduced to the BDT units for further optimization of material properties.[13] Based on these design rules, three different types of P_As [P(BDT2BOY5-X), x = H, F, Cl] are prepared, and show much higher absorption coefficients (ε^{max} = 1.11 × 10^5 cm^{-1}**)** and electron mobilities (μ_e = 1.6 × 10^{-4} cm^2 V^{-1} s^{-1}) compared to the conventional P(NDI2OD-T2) P_A (**Figure 1**). As a result, all-PSCs composed of PBDB-T:P(BDT2BOY5-X) blends have greatly enhanced PCEs (PCE = 11.12%) relative to P(NDI2OD-T2) (PCE = 6.00 %) or Y5-2BO NFSMA (PCE = 7.02 %) based PSCs. Importantly, due to the BDT units in both P(BDT2BOY5-X) P_As and PBDB-T P_D, PBDB-T:P(BDT2BOY5-X) blends show excellent molecular compatibility with a small $\gamma_{D\text{-}A}$ value of 0.3 – 0.4 mN m^{-1} compared to PBDB-T:P(NDI2OD-T2) ($\gamma_{D\text{-}A}$ = 1.64 mN m^{-1}) and PBDT-T:Y5-2BO ($\gamma_{D\text{-}A}$ = 2.21 mN m^{-1}) blends. This high compatibility results in enhanced thermal and mechanical properties of all-PSCs. For examples, the thermal stability at 100 ˚C of the PBDB-T:P(BDT2BOY5-Cl) all-PSC significantly outperforms the PBDB-T:Y5-2BO blend. The mechanical properties of the PBDB-T:P(BDT2BOY5-Cl) blend are also remarkably improved, showing a 7-fold increase of the COS (15.89%) and a 10-fold increase in toughness (3.24 MJ m^{-3}) over the of PBDB-T:Y5-2BO PSC (COS = 2.21% and toughness = 0.32 MJ m^{-3}). This work demonstrates the importance of molecular

compatibility in the P_A design for high performance, thermally stable, and mechanically robust all-PSCs.

2. Results and Discussion

2.1. Material Design and Optical/Electrochemical Properties

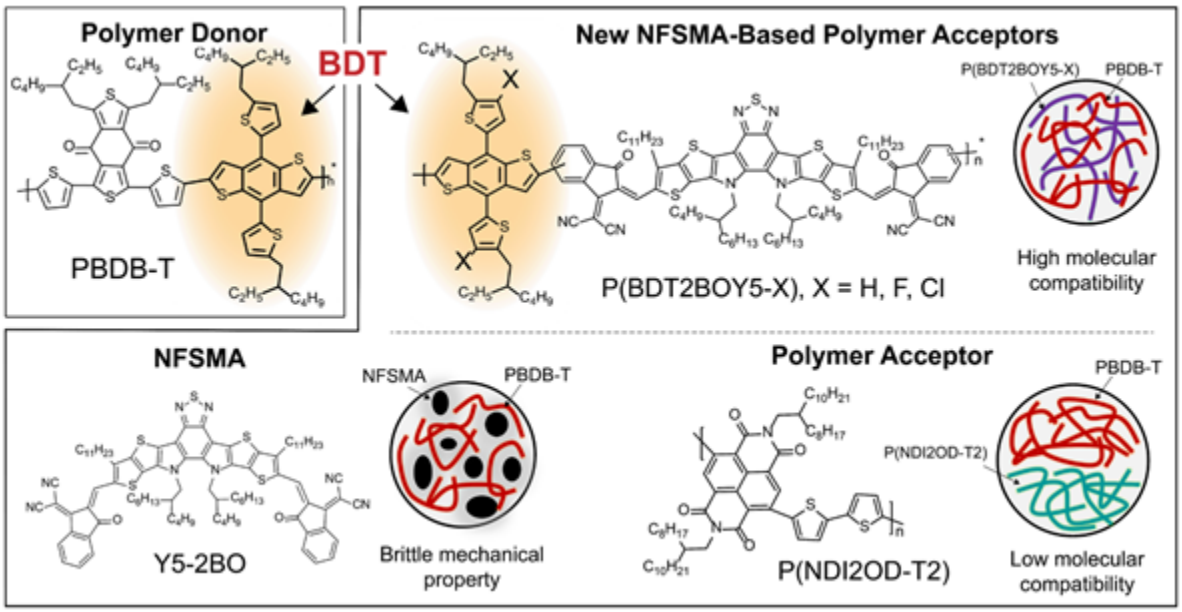

Figure 1. Chemical structures of the photovoltaic active materials used in this study; 1) PBDB-T donor, 2) a new series of NFSMA-based P_A materials P(BDT2BOY5-X), containing the same BDT building blocks of PBDB-T P_D, and 3) commonly used Y5-2BO NFSMA and P(NDI2OD-T2) P_A.

To develop efficient NFSMA-based P_As, a series of P_As [P(BDT2BOY5-X), X = H, F, Cl] (**Figure 1**) were designed with two major principles; i) polymerization of the NFSMA building blocks for enhanced light absorption, and ii) incorporation of the same monomer unit (*i.e.,* BDT) in both P_D and P_A backbones to generate favorable interfacial interactions that improve miscibility of the system. The 2,2'-((2*Z*,2'*Z*)-((12,13-bis(2-butyloctyl)-3,9-diundecyl-12,13-dihydro-[1,2,5]thiadiazolo[3,4-e]thieno[2'',3'':4',5']thieno[2',3':4,5]pyrrolo[3,2-g]thieno[2',3':4,5]thieno[3,2-*b*]indole-2,10-diyl)bis(methaneylylidene))bis(3-oxo-2,3-dihydro-1H-indene-2,1-diylidene))dimalononitrile (Y5-2BO) NFSMA was selected for its superior light absorption and charge mobility,[2a, 2b, 14] and the BDT moiety was used to increase molecular compatibility as it is widely used in many high performance P_Ds.[14-15] The BDT units were further functionalized with F and Cl halogens to tune the crystallinity of the resulting P_As.[13a, 16] With this molecular design, three different P(BDT2BOY5-X) P_As were prepared using a Stille coupling (**Scheme S3**)**.** The detailed synthetic procedures and characterizations for all chemical compounds in this study are described in the Supporting Information (**Figures S1-S8**). The obtained P(BDT2BOY5-X) P_As have number-average molecular weights (M_ns) between 12 – 14 kg

mol^{-1} and dispersities (*Đ*s) of ~1.8 (**Table 1** and **Figure S9**). These similar M_n values between the P_As allow for a direct comparison of the material properties independent of molecular weight effects. All-PSCs based on these P_As with a PBDB-T P_D were fabricated and their photovoltaic, thermal and mechanical properties were examined. Additionally, a NFSMA (Y5-2BO) and NDI-based P_A (poly[[*N*,*N*′-bis(2-octyldodecyl)-naphthalene-1,4,5,8-bis(dicarboximide)-2,6-diyl]-*alt*-5,5′-(2,2′-bithiophene)], P(NDI2OD-T2)) were included as reference electron acceptors to elucidate the effects of polymerization (P_A vs NFSMA) and different backbone moieties in the P_As (BDT vs others) on the photovoltaic and mechanical performances of the PSCs (**Figure 1**).

Table 1. Optical and electrochemical characteristics of materials.

Polymer	M_n (*Đ*) (kg mol^{-1})	$\lambda_{max}^{sol.}$ (nm)[a]	λ_{max}^{film} (nm)[b]	ε^{max} [× 10^5 cm^{-1}][c]	E_g^{opt} (eV)[d]	LUMO (eV)	HOMO (eV)
PBDB-T	46 (1.8)	615	619	0.76	1.80	-3.63[f]	-5.43[e]
P(BDT2BOY5-H)	12 (1.6)	766	789	1.11	1.45	-4.15[f]	-5.60[e]
P(BDT2BOY5-F)	12 (1.8)	771	789	1.12	1.45	-4.16[f]	-5.61[e]
P(BDT2BOY5-Cl)	14 (1.8)	775	789	1.11	1.44	-4.18[f]	-5.62[e]

Y5-2BO	–	721	816	1.05	1.40	-4.28[f)]	-5.68[e)]
P(NDI2OD-T2)	20 (2.2)	639	703	0.42	1.49	-4.31[f)]	-5.80[e)]

[a)] λ_{max} values of solution states in *ortho*-dichlorobenzene (*o*-DCB). [b)] λ_{max} values of film states. [c)]Absorption coefficients were calculated by the maximum absorption of the lower energy band in thin-film UV-Vis spectra. [d)]Optical band gaps were estimated from the absorption onsets in thin-films (spin-casted from 20 mg mL^{-1} *o*-DCB solutions). [e)]Measured by cyclic voltammetry. [f)]HOMO = LUMO − E_g^{opt}.

The basic optical and electrochemical properties of these materials were then characterized. The ultraviolet-visible (UV-Vis) absorption spectra and energy level alignments are displayed in **Figure S10**, and cyclic voltammograms are included in **Figure S11.** The detailed optical and electrochemical characteristics are summarized in **Table 1.** In **Figure S10a**, the P(BDT2BOY5-X) P_As show a red-shifted and increased absorbance in the intramolecular charge transfer (ICT) region (650 – 900 nm) compared to P(NDI2OD-T2) in their film states. Specifically, P(BDT2BOY5-X) P_As have a maximum film absorption wavelength (λ_{max}^{film}) of 789 nm with an absorption coefficient (ε^{max}) of 1.1 × 10^5 cm^{-1} compared to λ_{max}^{film} = 703 nm and ε^{max} = 0.4 × 10^5 cm^{-1} for P(NDI2OD-T2). The superior optical properties of the P(BDT2BOY5-X) P_As relative to P(NDI2OD-T2) are attributed to their highly fused ladder type backbone and the strong dye (*i. e.,* IC) unit,

similar to other NFSMAs or their P_A derivatives.[2a, 2b, 4a, 6, 17] The red-shifted and high ICT absorbance of P(BDT2BOY5-X) P_As is known to benefit charge generation due to increased photon absorption compared with NDI- or PDI-based P_As.[18] The P(BDT2BOY5-X) P_As show the linearly increasing maximum solution absorption wavelength ($\lambda_{max}^{sol.}$) values according to the sequential halogenations, while they show the identical λ_{max}^{film} value. For example, $\lambda_{max}^{sol.}$ increases from 766 nm of P(BDT2BOY5-H) to 771 nm of P(BDT2BOY5-F), and further increases to 775 nm of P(BDT2BOY5-Cl) (**Table 1**). This suggests the halogenation of the BDT units in the P_As accelerates pre-aggregation behaviors of the P_As, possibly due to enhanced backbone interactions. All of the acceptors show well-matched highest occupied molecular orbital/lowest unoccupied molecular orbital (HOMO/LUMO) energy levels with PBDB-T with enough offset for effective charge transfer (**Figure S10c**). The LUMO levels of P(BDT2BOY5-X) P_As (-4.18 to -4.15 eV) are upshifted compared with the Y5-2BO NFSMA (-4.28 eV), attributed to the incorporation of BDT donating units in P(BDT2BOY5-X). These upshifted LUMO levels for the P(BDT2BOY5-X) P_As drive larger bandgaps overlapped with PBDB-T compared to Y5-2BO and P(NDI2OD-T2), beneficial for producing a higher open-circuit voltage (V_{oc}) in PSC devices.

2.2. Photovoltaic Properties

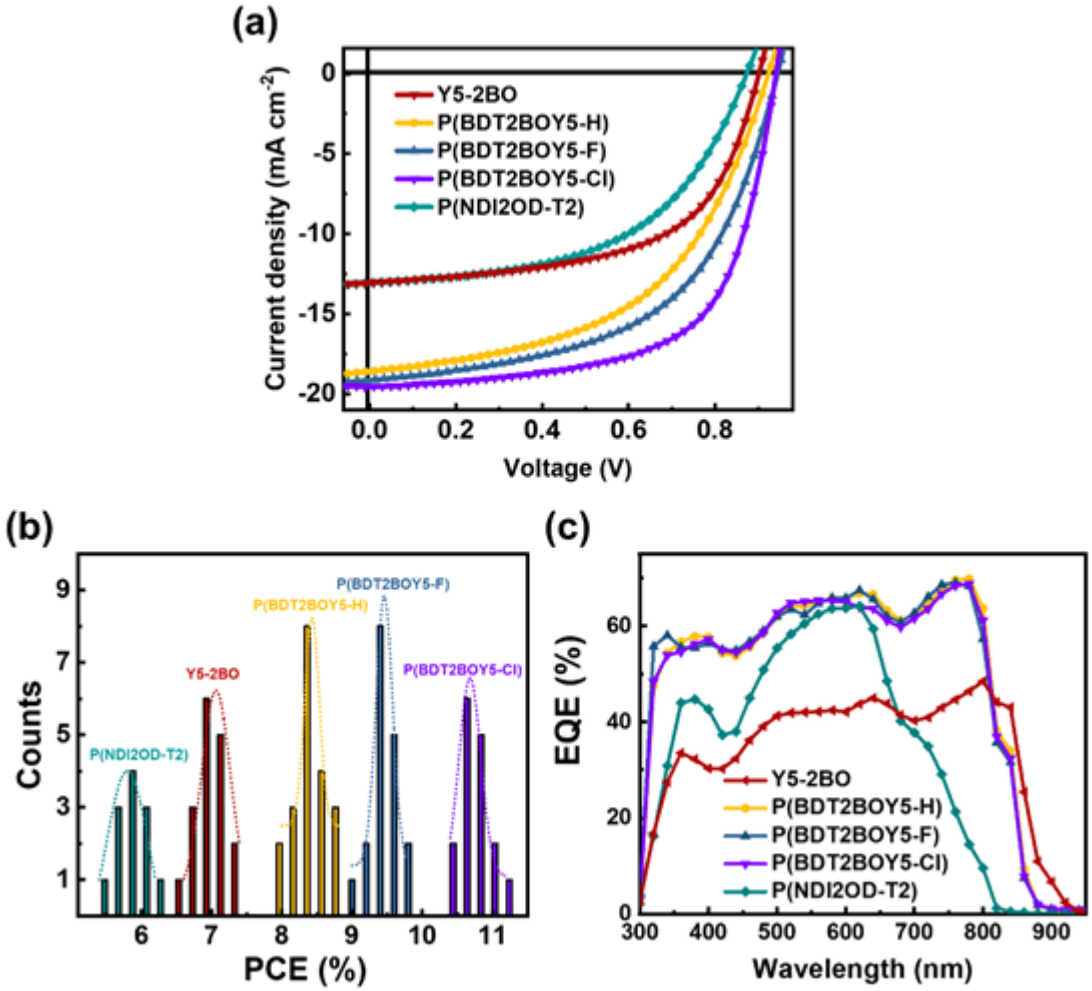

Figure 2. Photovoltaic performances of the PBDB-T: acceptor blends; a) *J-V* curves of the PSC devices, b) PCE-counts plots with Gaussian distributions, and c) EQE response spectra for the PBDB-T: acceptors.

Table 2. Photovoltaic performances of the PSC devices with PBDB-T:acceptor blends.

Acceptor	V_{oc} (V)[a)]	J_{sc} (mA/cm^2)[a)]	*Cal.* J_{sc} (mA/cm^2)	FF[a)]	$PCE_{avg(max)}$ (%)[a)]
P(BDT2BOY5-H)	0.92 ± 0.01	18.61 ± 0.17	18.43	0.51 ± 0.02	8.65 ± 0.14 (8.81)
P(BDT2BOY5-F)	0.92 ± 0.01	19.03 ± 0.23	18.57	0.55 ± 0.01	9.64 ± 0.15 (9.83)
P(BDT2BOY5-Cl)	0.92 ± 0.01	18.72 ± 0.24	18.54	0.63 ± 0.02	10.67 ± 0.17 (11.12)
Y5-2BO	0.89 ± 0.00	13.04 ± 0.11	12.72	0.60 ± 0.01	6.91 ± 0.09 (7.02)
P(NDI2OD-T2)	0.86 ± 0.01	13.08 ± 0.08	13.45	0.52 ± 0.02	5.86 ± 0.07 (6.00)

[a)]All of the parameters represent the average values measured from more than 10 devices.

Next, the photovoltaic properties of the PBDB-T:acceptor blends were investigated by fabricating PSC devices with a normal type device architecture. The detailed device fabrication conditions are described in the Experimental Section. **Figure 2** represents the

current density-voltage (*J-V*) curves, PCE-counts plot, and external quantum efficiency (EQE) response spectra for the PSC devices. The detailed photovoltaic parameters are summarized in **Table 2.** All of the PBDB-T:P(BDT2BOY5-X) blends show much higher PCEs compared to those of Y5-2BO NFSMA (PCE= 7.02 %) and P(NDI2OD-T2) systems (PCE= 6.00%) (**Figure 2a** and **Table 2**). The V_{oc} values of the PBDB-T:P(BDT2BOY5-X) blends are 0.03 - 0.06 V higher than other materials due to their upshifted LUMO levels relative to Y5-2BO and P(NDI2OD-T2). The higher PCEs for the PBDB-T:P(BDT2BOY5-X) compared to PBDB-T:P(NDI2OD-T2) are mainly attributed to the higher J_{sc}, resulted from the enhanced light absorption of P(BDT2BOY5-X). Among the PBDB-T:P(BDT2BOY5-X) blends, the PCE increases in the order of P(BDT2BOY5-H), P(BDT2BOY5-F), and P(BDT2BOY5-Cl), with maximum PCEs of 8.81, 9.83, and 11.12%, respectively. The main parameter determining the PCEs among the PBDB-T:P(BDT2BOY5-X) blends is the fill factor (FF), which will be discussed in the next section. We also added the counts versus PCE plots following Gaussian distributions for all blends in **Figure 2b**, which supports that all the PSC systems have reproducible performances with small deviations.

In the EQE response spectra in **Figure 2c**, the PBDB-T:Y5-2BO and PBDB-T:P(BDT2BOY5-X) blends show a wider EQE response range (300 to 900 nm) compared to

the PBDB-T:P(NDI2OD-T2) blend. This is attributed to the red-shifted absorbane for the Y5-2BO NFSMA and P(BDT2BOY5-X) P_As in the ICT region, achieving better complementary absorption with PBDB-T P_D compared to P(NDI2OD-T2).[18] Thus, the PBDB-T:P(BDT2BOY5-X) blends can generate higher currents in a wider absorption wavelength than the PBDB-T:P(NDI2OD-T2) blend. Additionally, the PBDB-T:Y5-2BO blend shows lower EQE responses throughout the total wavelength range in comparison to the PBDB-T:P(BDT2BOY5-X) blends. This indicates the lower J_{sc} of the PBDB-T:Y5-2BO blend is rooted in the charge transport or recombination process during PSC operation rather than the absorbance.

2.3. Charge Generation and Transport Properties

To gain a deeper insight into the FF and J_{sc} changes between devices, the charge mobilities for both the neat films and their blends were measured in the vertical direction by the space charge limited current (SCLC) method.[19] The pristine and blend SCLC mobilities are displayed in **Table S1** and **S2**, respectively. Among the acceptors, P(BDT2BOY5-X) polymer films show μ_e values from 5.6×10^{-5} to 1.6×10^{-4} $cm^2\ V^{-1}\ s^{-1}$

(**Table S1**). These μ_e values are 3 to 8-fold higher than the P(NDI2OD-T2) mobilities, indicating that the Y5-2BO NFSMA backbone is highly effective for enhancing charge transport in the resulting P_As. In the blends, all systems show comparable hole mobilities (μ_hs) around 2.1 – 2.6 × 10^{-4} cm^2 V^{-1} s^{-1}, since the same PBDB-T P_D is used for all the PSCs (**Table S2**). However, the μ_e values show notable differences between the blends, resulting in different hole/electron mobility balances (μ_h/μ_es) (**Table S2**). The μ_es of the PBDB-T:P(BDT2BOY5-X) blends increase in the order of P(BDT2BOY5-H), P(BDT2BOY5-F), and P(BDT2BOY5-Cl) from 4.7 × 10^{-5} to 1.4 × 10^{-4} cm^2 V^{-1} s^{-1}. Thus, the PBDB-T:P(BDT2BOY5-Cl) blend has the most balanced μ_h/μ_e value of 1.6, whereas the PBDB-T:P(BDT2BOY5-H) blend exhibits the highest μ_h/μ_e of 4.7. The μ_h/μ_e value is correlated with charge recombinations,[19] and explains the decreasing FF for P(BDT2BOY5-Cl) (FF = 0.63), P(BDT2BOY5-F) (FF = 0.55), and P(BDT2BOY5-H) (FF = 0.51) blends.

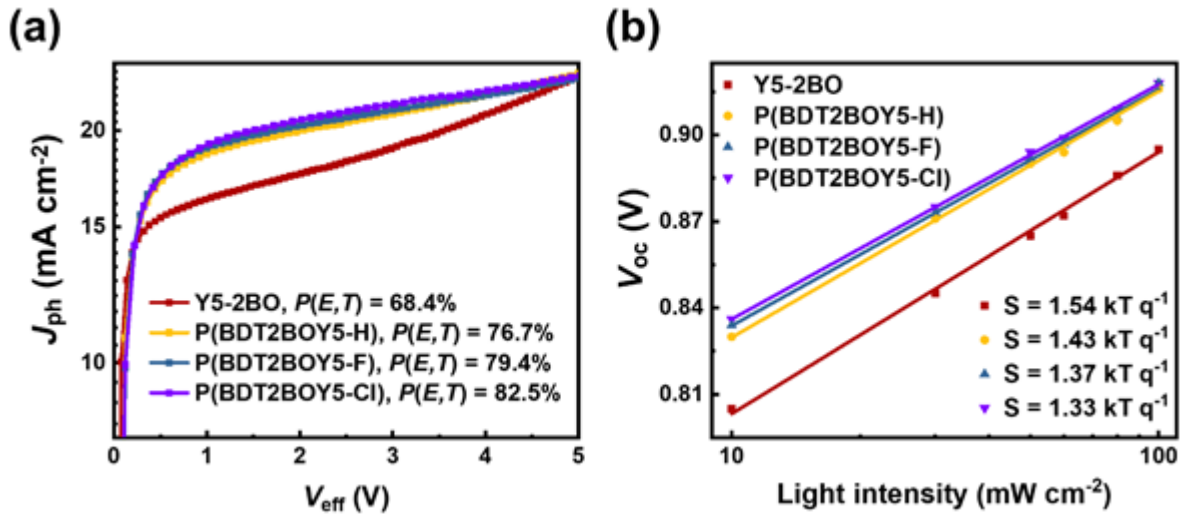

Figure 3. Analysis for the exciton dissociation and recombination properties of the PSCs; a) J_{ph}-V_{eff} curves for the PBDB-T:acceptor blends, and b) dependence of the V_{oc} on the light intensity for the PBDB-T:acceptor blends.

Next, we explored the exciton dissociation properties at donor-acceptor interfaces by measuring the photocurrent density (J_{ph}) under an effective voltage (V_{eff}).[20] **Figure 3a** displays the J_{ph}-V_{eff} curves of the PBDB-T:acceptor blends. The exciton dissociation probabilities ($P(E,T)$s) for the blends were calculated from the ratio between their J_{ph}s under short-circuit conditions and saturation current densities (J_{sat}s) at V_{eff} = 5V,[20] and are represented in the **Table S2**. The PBDB-T:Y5-2BO blend showed a much lower $P(E,T)$ (68.4%) than the other all-PSC blends. Additionally, the $P(E,T)$s of the P(BDT2BOY5-X) blends increased from 76.7% (PBDB-T:P(BDT2BOY5-H)), to 79.4% (PBDB-T:P(BDT2BOY5-

F)), and finally to 82.5% (PBDB-T:P(BDT2BOY5-Cl)), supporting the PCE trends for the all-PSCs. As a poor exciton dissociation lowers the J_{sc} of PSCs,[21] the low J_{sc} of PBDB-T:Y5-2BO compared to other blends can be explained by its inferior $P(E,T)$.

We also measured the light intensity (P) dependencies of J_{sc} and V_{oc} under optimal PSC device conditions to analyze the charge recombination properties with various acceptors (**Figure 3b** and **S12**). All the blends show similar α values between 0.82 to 0.84 in the J_{sc} vs light intensity relationships (**Figure S12**), suggesting there is no significant difference in bimolecular recombination among the blends.[22] It is also known the V_{oc} is proportional to the natural logarithm of P ($V_{oc} \propto \ln(P)$) in an open circuit condition, and the slope (S) with the unit of kT q^{-1} (k= Boltzmann constant, T= temperature, and q= elementary charge) approaches the unity when no monomolecular or trap-assisted recombination occurs.[23] In **Figure 3b**, the PBDB-T:Y5-2BO blend shows the strongest deviation (S = 1.54 kT q^{-1}) from the unity, indicating that PBDB-T:Y5-2BO suffers from severe monomolecular recombination of dissociated free charges during their transport to electrodes. Among the PBDB-T:P(BDT2BOY5-X) blends, the S values decrease linearly from 1.43 for PBDB-T: P(BDT2BOY5-H), 1.37 for PBDB-T: P(BDT2BOY5-F) and to 1.33 kT q^{-}

[1] for PBDB-T: P(BDT2BOY5-Cl). Thus, the trends of the monomolecular or trap-assisted recombination are consistent with the FF values of the all-PSCs.[24]

2.4. Morphological Properties

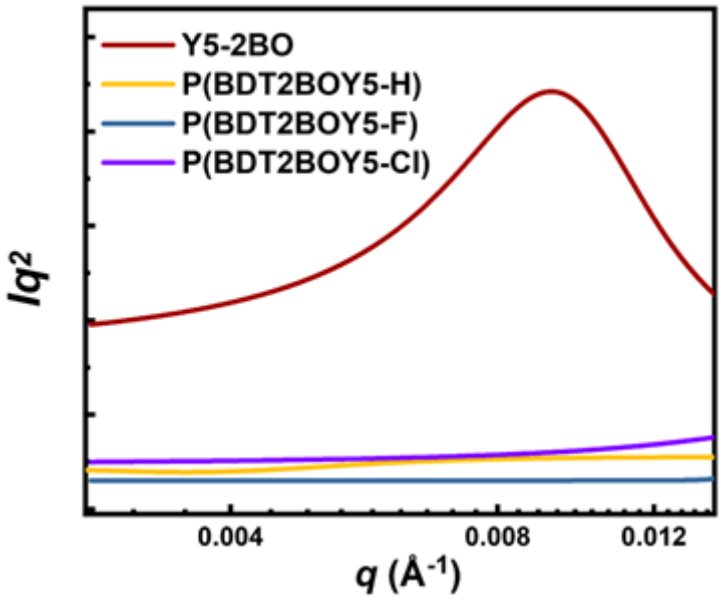

Figure 4. RSoXS intensity profiles of the PBDB-T:acceptor blends measured at 284.2 eV

Next, the resonant soft x-ray scattering (RSoXS) measurements for the PBDB-T:acceptor blends were performed to examine the degree of phase separation between the P_D and acceptors in the blends (**Figure 4**).[25] The photon energy of incidence light at 284.2 eV was selected to maximize material contrasts between the P_D and acceptors.[25a]

In **Figure 4**, clear differences exist among the blends depending on the acceptor materials. Whereas the PBDB-T:Y5-2BO blend shows a distinct peak at q = 0.0091 Å^{-1} (domain size= 69 nm), all the PBDB-T:P(BDT2BOY5-X) blends show no distinguishable peak. This finding indicates the phase separation between P_D and acceptors is suppressed in the PBDB-T:P(BDT2BOY5-X) blends. In contrast, the decreased donor-acceptor interfacial areas of the strongly-segregated PBDB-T:Y5-2BO domains support its inferior exciton dissociation and charge recombination properties observed in the prior section.[26] The PBDB-T:P(BDT2BOY5-X) blends have well-intermixed domains with larger donor-acceptor interfaces, benefitted from the high chemical compatibility between the P_D and P_A, which promotes exciton dissociation at the interfaces.

Table 3. Contact angles with water and glycerol and surface tensions of the materials, and interfacial tension between donor and acceptors.

Material	Θ_{water} (deg)	$\Theta_{glycerol}$ (deg)	Surface tension (mN m^{-1})	$\gamma_{D\text{-}A}$[a)] (mN m^{-1})
PBDB-T	100.4	87.4	24.6	-
P(BDT2BOY5-H)	94.8	80.5	28.3	**0.30**
P(BDT2BOY5-F)	95.0	80.1	28.9	**0.35**

P(BDT2BOY5-Cl)	94.5	79.4	29.4	**0.44**
Y5-2BO	97.8	79.9	32.6	**2.21**
P(NDI2OD-T2)	100.5	91.3	20.9	**1.64**

[a)] The interfacial tension between PBDB-T donor and acceptors.

To support the reduced phase-separation in the NSFMA based all-PSCs, the interfacial compatibility was investigated by measuring the contact angles of the materials using both water and glycerol droplets (**Table 3**). Then, the surface tension of the materials and interfacial tension ($\gamma_{D\text{-}A}$) between each donor and acceptor were calculated using the Wu model.[27] The experimental details for the contact angle measurement and calculation of $\gamma_{D\text{-}A}$ values are described in the Experimental Section. Interestingly, all the PBDB-T:P(BDT2BOY5-X) blends show lower $\gamma_{D\text{-}A}$ values (0.30 to 0.44 mN m^{-1}) compared to PBDB-T:P(NDI2OD-T2) ($\gamma_{D\text{-}A}$ = 1.64 mN m^{-1}) and PBDB-T:Y5-2BO ($\gamma_{D\text{-}A}$ = 2.21 mN m^{-1}) (**Table 3**). The low $\gamma_{D\text{-}A}$ value indicates high interfacial compatibility and a low enthalpy of mixing (ΔH_{mix}) between the donor and acceptor,[28] which suppresses their phase-separation to generate intermixed domains with large donor-

acceptor interfaces in the blends.[27] This finding supports the observations from earlier RSoXS experiment. We speculate that these low $\chi_{D\text{-}A}$ values of PBDB-T:P(BDT2BOY5-X) blends stem from the BDT units in the P_A backbones, having structural similarities to the PBDB-T donor. We believe these structural similarities are crucial to enhance the interfacial compatibility between the P_D and P_A and help produce an optimal blend morphology.

Additionally, the structural and morphological properties of the pristine and blend films were analyzed by grazing incidence x-ray scattering (GIXS) measurement (**Figure S13** and **S14**). The *d*-spacing and coherence length (L_c) of the out-of-plane (OOP) (010) peaks were calculated for both pristine and blend samples using the Scherrer equation (**Table S3** and **S4**).[29] Among the acceptor films, the Y5-2BO NFSMA shows the sharpest OOP (010) peak with the highest L_c of 35.4 Å and shortest *d*-spacing of 3.63 Å (**Figure S13** and **Table S3**), suggesting the NFSMA forms much larger crystals and tighter packings than the P_As. Among the P_As, the L_c value of the OOP (010) peaks increases in the order of P(BDT2BOY5-H) (L_c = 19.1 Å), P(BDT2BOY5-F) (19.9 Å), and P(BDT2BOY5-Cl) (23.7 Å). This indicates P_A crystallinity increases linearly with halogenation as previously reported,[13a, 13c, 30] and agrees with the pre-aggregation behaviors in the solution states in

UV-Vis analysis and pristine μ_e values in SCLC measurement. In the blend films, the PBDB-T:Y5-2BO blend shows the sharpest OOP (010) peak among all the blends with a L_c value of 25.3 Å at q = 1.72 $Å^{-1}$, suggesting the high crystallinity of the Y5-2BO NFSMA is retained in the blend (**Figure S14** and **Table S4**). Among the PBDB-T:P(BDT2BOY5-X) blends, L_c values of the OOP (010) peaks increase in the order of P(BDT2BOY5-H), P(BDT2BOY5-F), and P(BDT2BOY5-Cl), showing 16.7, 18.4, and 22.8 Å, respectively. This trend is well correlated with the increasing trend of the P_A crystallinity in the pristine films, which supports the increased blend SCLC μ_e and more balanced μ_h/μ_e results with halogenations in the previous section. To note, distinct peaks around q = 1.1 – 1.9 $Å^{-1}$ are observed in the in-plane (IP) direction for PBDB-T:Y5-2BO blend, corresponding to PBDB-T as shown in **Figure S13**. This suggests that the PBDB-T polymer retains its independent crystals separated from the Y5-2BO domains in the PBDB-T:Y5-2BO blend, caused by the high NFSMA crystallinity and low compatibility between the P_D and NFSMA. In contrast, the peaks from PBDB-T around q = 1.1 – 1.9 $Å^{-1}$ are not distinguishable in the PBDB-T:P(BDT2BOY5-X) blends. Thus, the formation of the separate aggregates of PBDB-T is suppressed, and intermixed domains of PBDB-T:P(BDT2BOY5-X)

are developed instead. This observation is consistent with the earlier RSoXS and interfacial tension results.

2.5. Mechanical Robustness and Thermal Stability

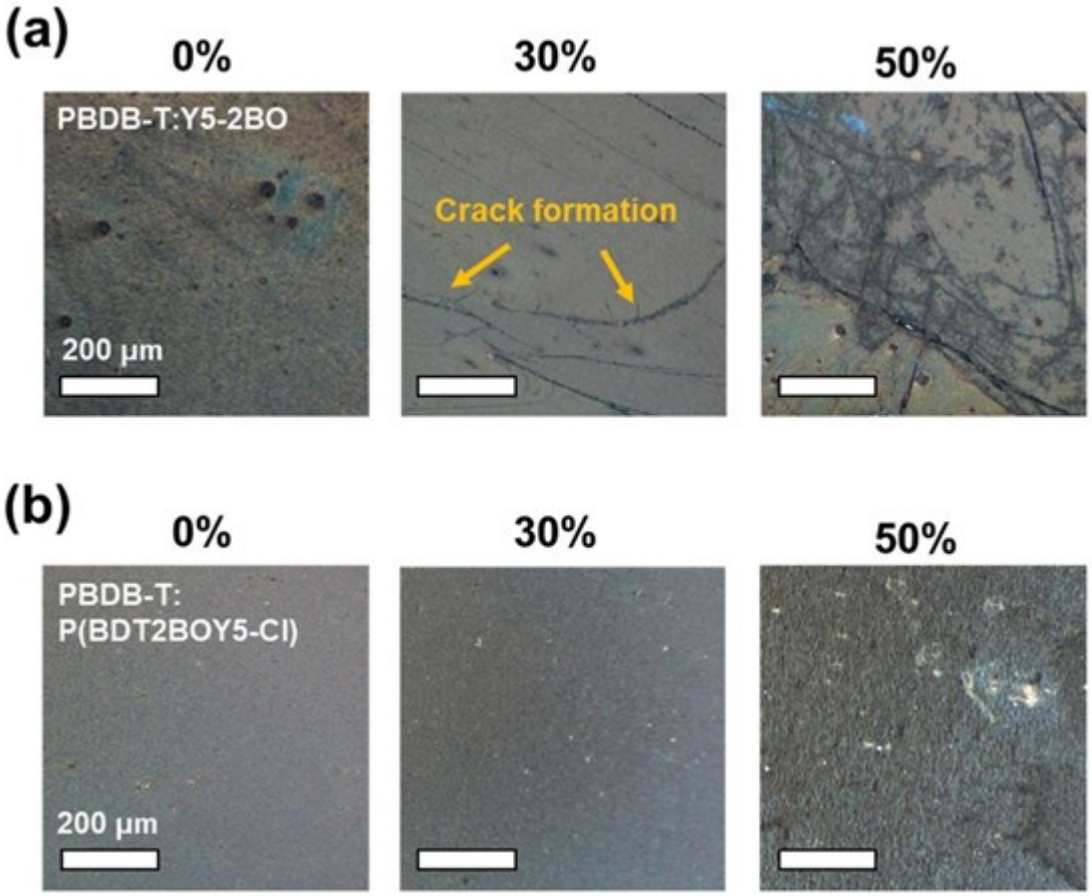

Figure 5. Optical microscopy images of the blend films on PDMS substrates under tensile strains; a) OM images for the PBDB-T:Y5-2BO blend, and b) OM images for the PBDB-T:P(BDT2BOY5-Cl) blend. the scale bar is 200 μm.

Next, we measured optical microscopy (OM) images of the PBDB-T:Y5-2BO and PBDB-T:P(BDT2BOY5-Cl) blends on poly(dimethylsiloxane) (PDMS) substrates with increasing tensile strain from 0 (unstrained) to 50% (**Figure 5**). Without any strain, the PBDB-T:Y5-2BO blend shows a rough morphology with many agglomerates on its surface due to the high crystallinity of Y5-2BO and strong immiscibility with the P_D. In contrast, the PBDB-T:P(BDT2BOY5-Cl) blend is very uniform without local aggregation compared with PBDB-T:Y5-2BO. Drastically different behaviors between the two blends are observed when external strain is applied. At 30% strain, many sharp cracks begin to propagate in the PBDB-T:Y5-2BO blend, while the PBDB-T:P(BDT2BOY5-Cl) blend remains uniform at the same strain. At 50% strain, more and larger cracks are developed in the PBDB-T:Y5-2BO blend, whereas only slight deformation of the initial morphology is observed in the PBDB-T:P(BDT2BOY5-Cl) film without any crack. This suggests that the PBDB-T:P(BDT2BOY5-Cl) blend has a much higher durability to mechanical stress compared with the PBDB-T:Y5-2BO blend.

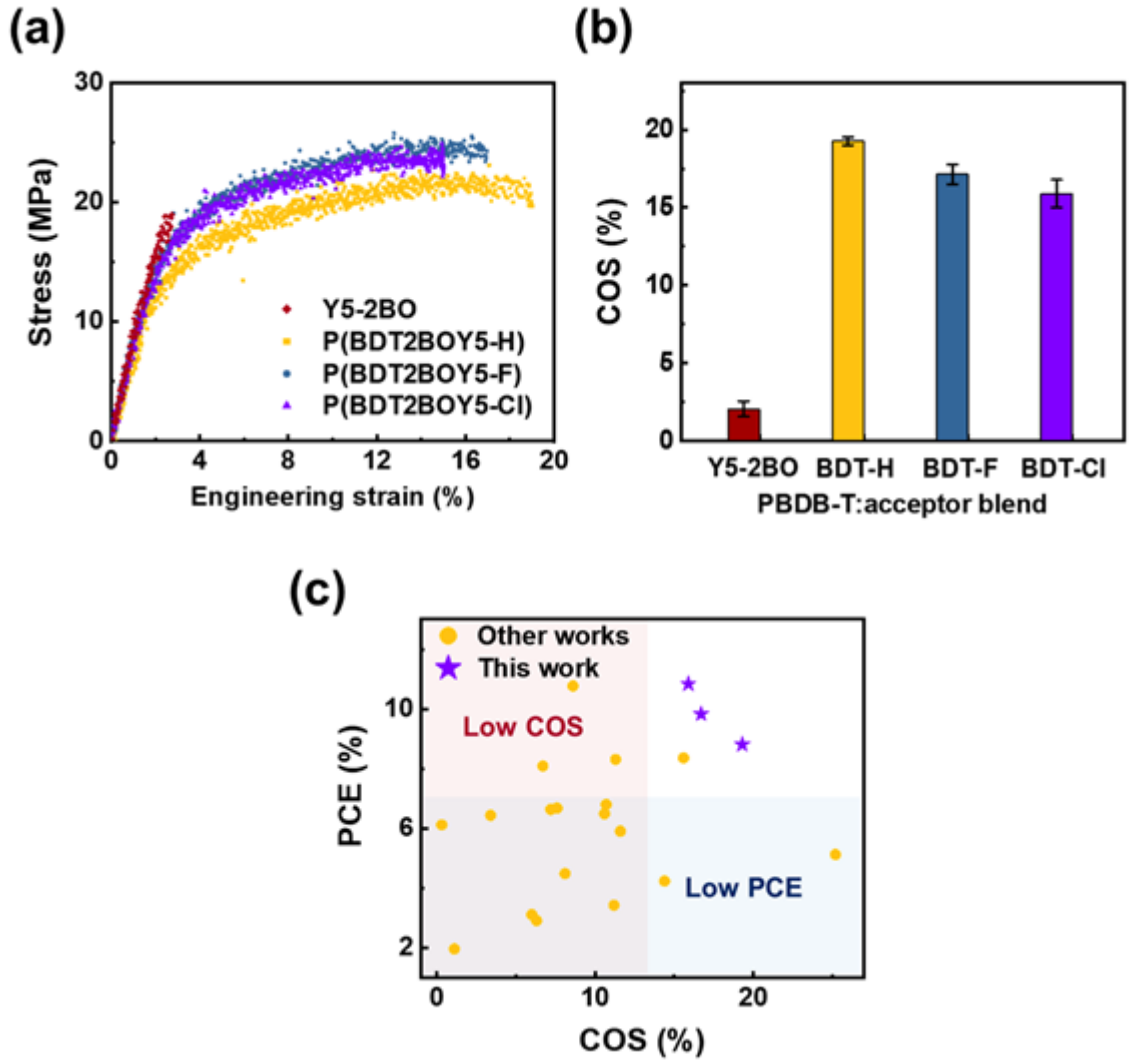

Figure 6. Pseudo free-standing tensile test results for the PBDB-T:acceptor blends; a) stress-strain curves, b) COS values of PBDB-T:acceptor blends depending on the acceptor materials, and c) summaries of PCE vs. COS (measured from pseudo free-standing tensile test) of the active layer blends in other works and this work.

Table 4. COS, toughness, and elastic modulus values for the PBDB-T:acceptor blends.

Acceptor	COS (%)	Toughness (MJ m^{-3})	Elastic modulus (GPa)
Y5-2BO	2.28 ± 0.48	0.32 ± 0.15	1.48 ± 0.09
P(BDT2BOY5-H)	19.27 ± 0.26	3.80 ± 0.37	0.75 ± 0.05
P(BDT2BOY5-F)	16.71 ± 0.26	3.51 ± 0.02	0.90 ± 0.04
P(BDT2BOY5-Cl)	15.89 ± 0.89	3.24 ± 0.33	0.82 ± 0.03

To develop a quantitative understanding of the mechanical properties of all-PSCs depending on acceptor types, the thin-film mechanical properties of both pristine and blend films were analyzed by a pseudo free-standing tensile test on a water surface. The pseudo free-standing tensile test can measure the intrinsic thin-film mechanical properties without any distortion caused by substrates.[31] The detailed sample structures and experimental methods are described in the Experimental Section. The measured stress-strain (*S*-*S*) curves of the blend thin-films are displayed in **Figure 6a**. The detailed mechanical values including COS, toughness, and elastic modulus for the pristine and blend films are represented in **Table S5** and **4**, respectively. To note, there exist significant differences between the PBDB-T:NFSMA and PBDB-T:P_A blends. Whereas the

PBDB-T:Y5-2BO blend shows brittle *S-S* behavior under tensile stress with a COS of 2.28%, all the PBDB-T:P(BDT2BOY5-X) blends show outstanding ductilities with COSs over 15% (**Figure 6b** and **Table 4**). Remarkably, the all-PSC blends show 7- and 10-times higher COS and toughness values compared to the NFSMA blend with the same donor, respectively. The superior ductilities of the PBDB-T:P(BDT2BOY5-X) blends are mainly driven by i) increased acceptor chain length by polymerization and ii) enhanced miscibility of P_As with P_D material from shared BDT units. The long P_A chains can interact with each other and bridge adjacent crystalline domains by forming tie molecules to dissipate external stress, unlike the NFSMA as previously reported.[4b, 12] Furthermore, the formation of well intermixed domains in the PBDB-T:P(BDT2BOY5-X) blends should also dissipate stress throughout the films. In contrast, we expect that the stress in the PBDB-T:Y5-2BO blend is highly concentrated into the fragile region around hard agglomerates driven by high crystallinity of NFSMA and its incompatibility with P_D. This result suggests that our new P_A design can enhance the mechanical robustness of the resulting active layers. Particularly, incorporating BDT units into the P(BDT2BOY5-X) backbone increases the P_D-P_A compatibility and dramatically improves both the PCE and mechanical properties relative to Y5-2BO NFSMA. Among the PBDB-T:P(BDT2BOY5-X) blends, the

COS slightly decreases in the order of P(BDT2BOY5-H) (COS = 19.3%), P(BDT2BOY5-F) (16.7%), and P(BDT2BOY5-Cl) (15.9%). This is attributed to increased crystallinity from halogenated BDT units as shown in GIXS results (**Figure S14**). The stress at the same strain increase in P(BDT2BOY5-F) and P(BDT2BOY5-Cl) blends compared with P(BDT2BOY5-H) due to hardness of the crystalline domains. It should be noted that the PBDB-T:P(BDT2BOY5-X) blends in this work achieved excellent PCE and COS values simultaneously, whereas most PSC blends in previous literatures observed a trade-off between these properties (**Figure 6c** and **Table S6**).[1a, 4, 7n, 32] This highlights the importance of our molecular design with strong potential for wearable and stretchable electronic applications.

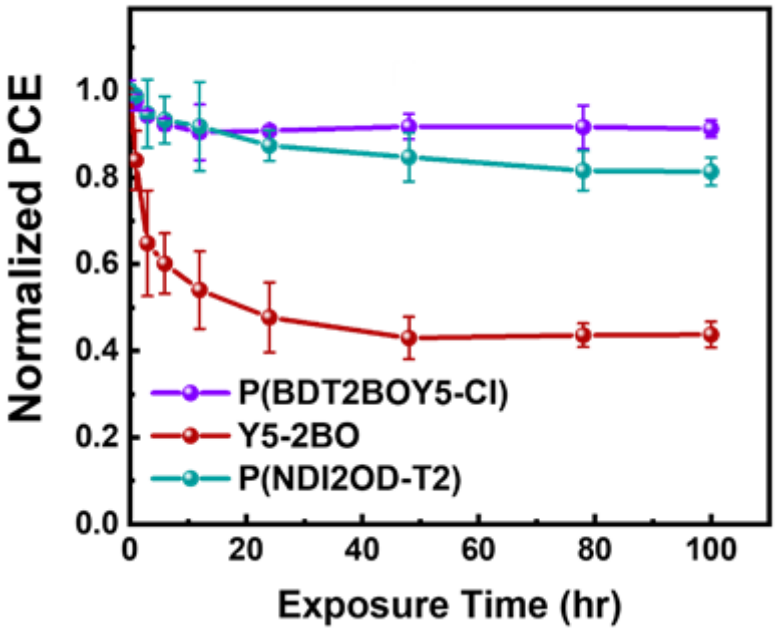

Figure 7. Normalized PCE versus exposure time (under 100 ^{0} C thermal stress) of the PBDB-T: acceptor blends.

Finally, the thermal stabilities of PBDB-T:P(BDT2BOY5-Cl), PBDB-T:Y5-2BO, and PBDB-T:P(NDI2OD-T2) PSCs at 100 °C were examined (**Figure 7**). A stark contrast in thermal stabilities was observed between the PBDB-T:Y5-2BO and PBDB-T:P_A systems. The electrical performance of the PBDB-T:Y5-2BO blend rapidly decreased at elevated temperatures with only 60 and 43% of the initial PCE after 6 and 48 hr, respectively. In contrast, the PBDB-T:P(BDT2BOY5-Cl) blend retained over 90% of its initial PCE even after

100 hr of heating (**Figure 7**). The PBDB-T:P(NDI2OD-T2) blend also exhibited much better thermal stability compared with that of the PBDB-T:Y5-2BO blend, maintaining 82% of the initial PCE after 100 hr. This result indicates the PBDB-T:P(BDT2BOY5-Cl) blend has superior morphological stabilities at high temperature relative to PBDB-T:Y5-2BO. The excellent thermal stability of the PBDB-T:P(BDT2BOY5-Cl) blend is mainly attributed to i) high molecular compatibility between P_D and P_A ,[33] and ii) low diffusion kinetics of P_A chains from entropic restraints.[6] Therefore, the mechanical robustness and thermal stability of all-PSCs can be significantly enhanced by carefully designing the P_A to have a high molecular compatibility with the P_D.

3. Conclusion

In conclusion, we successfully developed both highly efficient, mechanically and thermally-robust all-PSC systems with novel P(BDT2BOY5-X) P_A series, by dramatic enhancement of material compatibility between P_D and P_A. These new P_As have greatly enhanced absorption coefficients and electron mobilities compared to existing NDI-based P_As. For example, P(BDT2BOY5-Cl) showed 3- and 8-times higher μ_e and ε^{max} values relative with P(NDI2OD-T2). Remarkable material compatibility was achieved when

these P(BDT2BOY5-X) P_As containing BDT units were blended with BDT-based P_Ds. All-PSCs based PBDB-T and P(BDT2BOY5-X) blends showed high PCEs (up to 11.12%) that outperform the devices based on existing electron NFSMAs (PCE = 7.02%) and P(NDI2OD-T2) (PCE = 6.00%). Additionally, the P(BDT2BOY5-Cl)-based all-PSC displayed a much higher thermal stability at an elevated temperature (at 100 ^{0} C) compared to the Y5-2BO-based device. Moreover, excellent mechanical robustness has been realized in these blends of PBDB-T and P(BDT2BOY5-X). For instance, PBDB-T: P(BDT2BOY5-Cl) had a 7- and 10-times higher crack onset strain (COS) of 15.9% and toughness of 3.24 MJ m^{-3} in comparison with PBDB-T:Y5-2BO. These simultaneous improvements of the photovoltaic performance, thermal stability, and mechanical ductility are a result of the enhanced molecular compatibility between structurally similar P_D and P_As. This work provides important and simple design guidelines for the development of highly efficient and stretchable all-PSCs, paving the way for practical wearable or foldable power generators.

4. Experimental Section

Materials: The PBDB-T P_D was purchased by Brilliant Matters. The M_n and $Đ$ of the PBDB-T is mearsured by GPC analysis using the *1,2,4*-trichlorobenzene eluent at 150 °C. P(NDI2OD-T2) was polymerized by Stille polycondensation of 4,9-dibromo-2,7-bis(2-octyldodecyl)benzo[lmn][3,8]-phenanthroline-1,3,6,8-tetraone (NDIOD-2Br) and 5,5-bis(trimethylstannyl)-2,2-bithiophene, following the previous report.[7n] PNDITF3N-Br was synthesized by Suzuki–Miyaura cross-coupling reaction of comonomers, N,N′-bis(2-ethylhexyl)-2,6-bis(5-bromo-thiophen-2-yl)-1,4,5,8-naphthalenediimide and 2,7-bis(4,4,5,5-tetramethyl-1,3,2-dioxaborolane-2-yl)-9,9-bis(6-(N,N-dimethylamino)-propyl)fluorine. Then quaternization was proceeded by bromoethane according to the previously reported method.[34] INCN-Br, 2,5-bis(trimethylstannyl)thiophene, (4,8-bis(5-(2-ethylhexyl)thiophen-2-yl)benzo[1,2-b:4,5-b']dithiophene-2,6-diyl)bis(trimethylstannane) , (4,8-bis(5-(2-ethylhexyl)-4-fluorothiophen-2-yl)benzo[1,2-b:4,5-b']dithiophene-2,6-diyl)bis(trimethylstannane), and (4,8-bis(4-chloro-5-(2-ethylhexyl)thiophen-2-yl)benzo[1,2-b:4,5-b']dithiophene-2,6-diyl)bis(trimethylstannane) were purchased from Solarmer Materials Inc. Monomers used in the polycondensations were purchased from Sunatech Incorporation. All the other eluents and reagents were purchased from Sigma-Aldrich.

Synthesis: Detailed synthetic routes and chemical composition of the NFSMA and P_As are described in the Supporting Information.

Characterizations: Bruker Avance-300 MHz and Bruker 500 FT-NMR spectrometers were used to measure ^{1}H-NMR spectra, and the chemical shifts in the spectra have units of ppm. A SCIEX 4800 mass spectrometer was performed with a dithranol as matrix. A UV-1650PC spectrophotometer was used for the UV− Vis absorption spectra. The ε^{max} values of the materials were based on the maximum absorption in the ICT region, and calculated using the Beer-Lambert law; A = εd where A is absorbance, d is film thickness. Atomic force microscopy (AFM, Veeco Dimension 3100) was used to analyze the film thicknesses. An EG and G Parc model 273 Å potentiostat/galvanostat system was used for cyclic voltammetry measurements, having a three-electrode cell with tetrabutylammonium perchrolate in chloroform (0.1 M) at a scan rate of 50 mV s^{-1}. The M_n and $Đ$ of polymers except for PBDB-T were determined by GPC analysis with an Agilent GPC 1200 instrument equipped with a refractive index detector, in condition of

o-DCB eluent at 80 ℃ with polystyrene standards. The films for the OM measurement were spin-casted onto the polystyrenesulfonate (PSS)-coated glass, and then transferred to the PDMS substrates. GIXS analysis was conducted in the Pohang Accelerator Laboratory (beamline 9A, Republic of Korea), with incidence angle between 0.12 - 0.14°. L_c values of the materials were calculated using Scherrer equation :

$$L_c = \frac{2\pi K}{\Delta_q}$$

(K (shape factor) = 0.9 and Δ_q = full width half maximum (FWHM) of the scatterings)

PSC Fabrication: The PSCs with a normal architecture (ITO/PEDOT:PSS/active layer/PNDITF3N-Br/Ag) were prepared with the following procedures. ITO-coated glass substrates were treated by ultrasonication with deionized water, acetone, and isopropyl alcohol. Then, the ITO substrates were dried for 6 h in a hot oven (70 °C) at an ambient condition and then plasma treated for 10 min. Spincoating of the PEDOT:PSS solution (Clevios, AI4083) was done at 3000 RPM for 30 s onto the ITO substrates and, then, the substrates were annealed in air (165 °C, 30 min) before moving to an N_2-filled glovebox. The active layer solutions of PBDB-T P_D and acceptor materials with optimal

concentrations (18 mg mL^{-1} for PBDB-T:P(BDT2BOY5-X), 24 mg mL^{-1} for PBDB-T:Y5-2BO, and 16 mg mL^{-1} for PBDB-T:P(NDI2OD-T2)), donor:acceptor weight ratio (1:1), and solvent additive (2-chloronaphtalene, 3 vol%) were dissolved together in *o*-DCB, and then heated for 2 h on a 110 ℃ plate. The solution was spin-casted onto the PEDOT:PSS layer at 1000 rpm and 150 s, and, then, the samples were dried with high vacuum (< 10^{-5} torr) for 30 min. The samples were annealed at 120 ℃ for 10 min. Then, the PNDITF3N-Br of 1mg mL^{-1} in methanol was spin-casted with the condition of 2500 rpm for 30 s. Finally, Ag (120 nm) was deposited under high vacuum (~10^{-6} Torr) in an evaporation chamber. OM was used to measure the exact photoactive area of the devices (0.164 cm^2), and Keithley 2400 SMU instrument was used to measure the PSC efficiency under an air mass 1.5 G solar simulator (100 mW cm^{-2}, solar simulator: K201 LAB55, McScience), satisfying the Class AAA, ASTM Standards. K801SK302 of McScience was used as a standard silicon reference cell to calibrate the exact solar intensity. K3100 IQX, McScience Inc. instrument was used to analyze the EQE response spectra, equipped with a monochromator (Newport) and an optical chopper (MC 2000 Thorlabs).

SCLC Measurement: Both the pristine and blend charge carrier mobilities were calculated by the SCLC method. The electron- and hole-only devices were fabricated with device structures of ITO/ZnO/active layer/LiF/Al and ITO/PEDOT:PSS/active layer/Au, respectively. The semiconducting layers were prepared in the same condition with PSC fabrication, and the measured *J-V* characteristics were fitted to the Mott-Gurney equation:

$$J_{SCLC} = \frac{9}{8}\varepsilon_0\varepsilon_r\mu(V^2L^{-3}).$$

(ε_0 = free-space permittivity, ε_r = dielectric constant of the semiconductor, μ = is the charge carrier mobility, V = applied voltage, and L = thickness of the active layer.)

Contact Angle Measurements and Interfacial Tension Calculation: A Contact Angle Analyzer (Phoenix 150, SEO, Korea) was used to measure contact angles of the materials. The surface tension of the thin-films were calculated by the Wu model, using both the contact angles from water and glycerol (GC) on films. The detailed calculation method is described below:

$$\gamma_{\text{water}}(1+\cos\theta_{\text{water}}) = \frac{4\gamma^{\text{d}}_{\text{water}}\gamma^{\text{d}}}{4\gamma^{\text{d}}_{\text{water}} + 4\gamma^{\text{d}}} + \frac{4\gamma^{\text{p}}_{\text{water}}\gamma^{\text{p}}}{4\gamma^{\text{p}}_{\text{water}} + 4\gamma^{\text{p}}} \quad (1)$$

$$\gamma_{GC}(1+\cos\theta_{GC}) = \frac{4\gamma_{GC}^{d}\gamma^{d}}{4\gamma_{GC}^{d}+4\gamma^{d}} + \frac{4\gamma_{GC}^{p}\gamma^{p}}{4\gamma_{GC}^{p}+4\gamma^{p}} \quad (2)$$

$$\gamma_{total} = \gamma^{d} + \gamma^{p} \quad (3)$$

(γ^{total} = total surface tension, γ^{d} = dispersion component, γ^{p} = polar component, θ is the contact angle of water or GC.)

Then, the interfacial tension between P_D and acceptors were calculated based on the surface tensions, following the calculation below:

$$\gamma_{12} = \gamma_1 + \gamma_2 - \frac{4\gamma_1^{d}\gamma_2^{d}}{\gamma_1^{d}+\gamma_2^{d}} - \frac{4\gamma_1^{p}\gamma_2^{p}}{\gamma_1^{p}+\gamma_2^{p}} \quad (4)$$

(γ_{12} = interfacial tension between two different materials, γ_j (j = 1 or 2) = surface tension of each material, γ_j^{d} = dispersion component of the surface tension, γ_j^{p} = polar component of the surface tension)

Pseudo-freestanding tensile test: For the tensile test, acceptor, PBDB-T or blend solutions were spin-coated on the PSS-coated ITO glass substrates under the same coating conditions to the PSC fabrication. To prevent any fracture of the films at the grips, a femtosecond laser was used to cut the coated films on the PSS-coated ITO glass substrate into a dog-bone shape. By submerging the ITO glass substrate, the films were floated on the deionized water surface as PSS dissolved in the water. Subsequently, the

floated film was gripped to the PDMS-coated aluminum grips by van der Waals adhesion. In the tensile tests, applied strain rate was constant at ~ 0.8 × 10^{-3} s^{-1}. The tensile load values for each strain were measured to obtain stress-strain curves by using load cell with high resolution (LTS-10GA, KYOWA, Japan). All of tensile tests were carried out under the ambient conditions (temperature ~ 25 °C, relative humidity ~ 30 %). Detailed procedure for calculation of COS and toughness was explained in our previous reports.[4b, 7n]

Supporting Information

Synthetic routes and chemical structure confirmations of NFSMA and P_As, UV-Vis spectra, cyclic voltammograms, dependence on light intensity of J_{sc}, GIXS analysis, and pristine mechanical properties are included in the Supporting Information. Supporting Information is available from the Wiley Online Library or from the author.

Acknowledgements

J.-W. Lee and C. Sun contributed equally in this work. This work is supported by National Research Foundation of Korea (NRF) Grant of the Korean Government (No. 2020M3D1A2102756, 2020M3D1A2102869, 2020M3H4A1A01086888 and 2018R1A2A1A05078734). This work is also supported by Korea Institute of Energy Technology Evaluation and Planning (KETEP) Grant (No. 20173010013000) of the Korean Government. The experiment at Advanced Light Source is supported by a DOE office of Science User Facility under contract no. DE-AC02-05CH11231.

Received: ((will be filled in by the editorial staff))
Revised: ((will be filled in by the editorial staff))
Published online: ((will be filled in by the editorial staff))

References

[1] a) T. Kim, J. H. Kim, T. E. Kang, C. Lee, H. Kang, M. Shin, C. Wang, B. W. Ma, U. Jeong, T. S. Kim, B. J. Kim, *Nat. Commun.* **2015**, *6*, 8547; b) M. Kaltenbrunner, M. S. White, E. D. Glowacki, T. Sekitani, T. Someya, N. S. Sariciftci, S. Bauer, *Nat. Commun.* **2012**, *3*, 770; c) D. J. Lipomi, B. C. K. Tee, M. Vosgueritchian, Z. N. Bao, *Adv. Mater.* **2011**, *23*, 1771.

[2] a) Y. Cui, H. F. Yao, J. Q. Zhang, T. Zhang, Y. M. Wang, L. Hong, K. H. Xian, B. W. Xu, S. Q. Zhang, J. Peng, Z. X. Wei, F. Gao, J. H. Hou, *Nat. Commun.* **2019**, *10*, 2515; b) J. Yuan, Y. Q. Zhang, L. Y. Zhou, G. C. Zhang, H. L. Yip, T. K. Lau, X. H. Lu, C. Zhu, H. J. Peng, P. A. Johnson, M. Leclerc, Y. Cao, J. Ulanski, Y. F. Li, Y. P. Zou, *Joule* **2019**, *3*, 1140; c) A. Wadsworth, M. Moser, A. Marks, M. S. Little, N. Gasparini, C. J. Brabec, D. Baran, I. McCulloch, *Chem. Soc. Rev.* **2019**, *48*, 1596; d) H. Sun, F. Chen, Z. K. Chen, *Mater. Today* **2019**, *24*, 94; e) C. Zhu, J. Yuan, F. Cai, L. Meng, H. Zhang, H. Chen, J. Li, B. Qiu, H. Peng, S. Chen, Y. Hu, C. Yang, F. Gao, Y. Zou, Y. Li, *Energy Environ. Sci.* **2020**, *13*, 2459.

[3] F. F. Cai, C. Zhu, J. Yuan, Z. Li, L. Meng, W. Liu, H. J. Peng, L. H. Jiang, Y. F. Li, Y. P. Zou, *Chem. Commun.* **2020**, *56*, 4340.

[4] a) Q. P. Fan, W. Y. Su, S. S. Chen, W. Kim, X. B. Chen, B. Lee, T. Liu, U. A. Mendez-Romero, R. J. Ma, T. Yang, W. L. Zhuang, Y. Li, Y. W. Li, T. S. Kim, L. T. Hou, C. Yang, H. Yan, D. H. Yu, E. G. Wang, *Joule* **2020**, *4*, 658; b) J. Choi, W. Kim, S. Kim, T. S. Kim, B. J. Kim, *Chem. Mater.* **2019**, *31*, 9057.

[5] F. C. Krebs, T. D. Nielsen, J. Fyenbo, M. Wadstrom, M. S. Pedersen, *Energy Environ. Sci.* **2010**, *3*, 512.

[6] Q. Fan, w. Su, S. Chen, T. Liu, W. Zhuang, R. Ma, X. Wen, Z. Yin, Z. Luo, X. Guo, L. Hou, K. Moth-Poulsen, Y. Li, Z. Zhang, C. Yang, D. Yu, H. Yan, M. Zhang, E. Wang, *Angew. Chem. Int. Ed. DOI:10.1002/anie.202005662*.

[7] a) S. S. Chen, S. Jung, H. J. Cho, N. H. Kim, S. Jung, J. Q. Xu, J. Oh, Y. Cho, H. Kim, B. Lee, Y. An, C. F. Zhang, M. Xiao, H. Ki, Z. G. Zhang, J. Y. Kim, Y. F. Li, H. Park, C. Yang, *Angew. Chem. Int. Ed.* **2018**, *57*, 13277; b) H. T. Yao, F. J. Bai, H. W. Hu, L. Arunagiri, J. Q. Zhang, Y. Z. Chen, H. Yu, S. S. Chen, T. Liu, J. Y. L. Lai, Y. P. Zou, H. Ade, H. Yan, *ACS Energy Lett.* **2019**, *4*, 417; c) Y. J. Hwang, T. Earmme, B. A. E. Courtright, F. N. Eberle, S. A. Jenekhe, *J. Am. Chem. Soc.* **2015**, *137*, 4424; d) H. Benten, T. Nishida, D. Mori, H. J. Xu, H. Ohkita, S. Ito, *Energy Environ. Sci.* **2016**, *9*, 135; e) N. J. Zhou, A. S. Dudnik, T. I. N. G. Li, E. F. Manley, T. J. Aldrich, P. J. Guo, H. C. Liao, Z. H. Chen, L. X. Chen, R. P. H. Chang, A. Facchetti, M. O. de la Cruz, T. J. Marks, *J. Am. Chem. Soc.* **2016**, *138*, 1240; f) Y. K. Guo, Y. K. Li, O. Awartani, H. Han, J. B. Zhao, H. Ade, H. Yan, D. H. Zhao, *Adv. Mater.* **2017**, *29*, 1700309; g) W. Wang, Q. Wu, R. Sun, J. Guo, Y. Wu, M. M. Shi, W. Y. Yang, H. N. Li, J. Min, *Joule* **2020**, *4*, 1070; h) Z. G. Zhang, Y. K. Yang, J. Yao, L. W. Xue, S. S. Chen, X. J. Li, W. Morrison, C. Yang, Y. F. Li, *Angew. Chem. Int. Ed.* **2017**, *56*, 13503; i) R. Y. Zhao, N. Wang, Y. J. Yu, J. Liu, *Chem. Mater.* **2020**, *32*, 1308; j) X. J. Long, Z. C. Ding, C. D. Dou, J. D. Zhang, J. Liu, L. X. Wang, *Adv. Mater.* **2016**, *28*, 6504; k) H. L. Sun, Y. M. Tang, C. W. Koh, S. H. Ling, R. Z. Wang, K. Yang, J. W. Yu, Y. Q. Shi, Y. F. Wang, H. Y. Woo, X. G. Guo, *Adv. Mater.* **2019**, *31*, 1807220; l) M. Kim, H. I. Kim, S. U. Ryu, S. Y. Son, S. A. Park, N. Khan, W. S. Shin, C. E. Song, T. Park, *Chem. Mater.* **2019**, *31*, 5047; m) X. Liu, C. H. Zhang, C. H. Duan, M. M. Li, Z. C. Hu, J. Wang, F. Liu, N. Li, C. J. Brabec, R. A. J. Janssen, G. C. Bazan, F. Huang, Y. Cao, *J. Am. Chem. Soc.* **2018**, *140*, 8934; n) J.-W. Lee, B. S. Ma, J. Choi, J. Lee, S. Lee, K. Liao, W. Lee, T. S. Kim, B. J. Kim, *Chem. Mater.* **2020**, *32*, 582; o) Y. N. Zhang, Y. L. Xu, M. J. Ford, F. C. Li, J. X. Sun, X. F. Ling, Y. J. Wang, J. N. Gu, J. Y. Yuan, W. L. Ma, *Adv. Energy Mater.* **2018**, *8*, 1800029; p) T. Kim, R. Younts, W. Lee, S. Lee, K. Gundogdu, B. J. Kim, *J. Mater. Chem. A* **2017**, *5*, 22170; q) T. Kim, J. Choi, H. J. Kim, W. Lee, B. J.

Kim, *Macromolecules* **2017**, *50*, 6861; r) C. Lee, S. Lee, G. U. Kim, W. Lee, B. J. Kim, *Chem. Rev.* **2019**, *119*, 8028; s) K. Feng, J. C. Huang, X. H. Zhang, Z. Wu, S. B. Shi, L. Thomsen, Y. Q. Tian, H. Y. Woo, C. R. McNeill, X. G. Guo, *Adv. Mater.* **2020**, *32*, 2001476; t) Z. Genene, W. Mammo, E. G. Wang, M. R. Andersson, *Adv. Mater.* **2019**, *31*, 1807275; u) J.-W. Lee, M. J. Sung, D. Kim, S. Lee, H. You, F. S. Kim, Y. H. Kim, B. J. Kim, S. K. Kwon, *Chem. Mater.* **2020**, *32*, 2572.

[8] a) S. H. Shi, J. Y. Yuan, G. Q. Ding, M. Ford, K. Y. Lu, G. Z. Shi, J. X. Sun, X. F. Ling, Y. Li, W. L. Ma, *Adv. Funct. Mater.* **2016**, *26*, 5669; b) J. Yang, B. Xiao, A. L. Tang, J. F. Li, X. C. Wang, E. J. Zhou, *Adv. Mater.* **2019**, *31*, 1804699.

[9] J. Q. Du, K. Hu, L. Meng, I. Angunawela, J. Y. Zhang, S. C. Qin, A. Liebman-Pelaez, C. H. Zhu, Z. J. Zhang, H. Ade, Y. F. Li, *Angew. Chem. Int. Ed.* **2020**, *59*, 15181.

[10] a) N. Wang, X. J. Long, Z. C. Ding, J. R. Feng, B. J. Lin, W. Ma, C. D. Dou, J. Liu, L. X. Wang, *Macromolecules* **2019**, *52*, 2402; b) N. Wang, Y. J. Yu, R. Y. Zhao, Z. C. Ding, J. Liu, L. X. Wang, *Macromolecules* **2020**, *53*, 3325.

[11] D. D. Liu, J. M. Prausnitz, *Macromolecules* **1979**, *12*, 454.

[12] N. Balar, J. J. Rech, R. Henry, L. Ye, H. Ade, W. You, B. T. O'Connor, *Chem. Mater.* **2019**, *31*, 5124.

[13] a) H. F. Yao, J. W. Wang, Y. Xu, S. Q. Zhang, J. H. Hou, *Acc. Chem. Res.* **2020**, *53*, 822; b) H. F. Meng, Y. C. Li, B. Pang, Y. Q. Li, Y. Xiang, L. Guo, X. M. Li, C. L. Zhan, J. H. Huang, *ACS Appl. Mater. Interfaces* **2020**, *12*, 2733; c) Q. Q. Zhang, M. A. Kelly, N. Bauer, W. You, *Acc. Chem. Res.* **2017**, *50*, 2401.

[14] J. Yuan, Y. Q. Zhang, L. Y. Zhou, C. J. Zhang, T. K. Lau, G. C. Zhang, X. H. Lu, H. L. Yip, S. K. So, S. Beaupre, M. Mainville, P. A. Johnson, M. Leclerc, H. G. Chen, H. J. Peng, Y. F. Li, Y. P. Zou, *Adv. Mater.* **2019**, *31*, 1807577.

[15] H. T. Fu, Z. H. Wang, Y. M. Sun, *Angew. Chem. Int. Ed.* **2019**, *58*, 4442.

[16] G. P. Kini, S. J. Jeon, D. K. Moon, *Adv. Mater.* **2020**, *32*, 1906175.

[17] X. Ke, L. Meng, X. Wan, Y. Cai, H.-H. Gao, Y.-Q.-Q. Yi, Z. Guo, H. Zhang, C. Li, Y. Chen, *Nano Energy* **2020**, *75*, 104988.

[18] H. J. Bin, Y. K. Yang, Z. G. Zhang, L. Ye, M. Ghasem, S. S. Chen, Y. D. Zhang, C. F. Zhang, C. K. Sun, L. W. Xue, C. D. Yang, H. Ade, Y. F. Li, *J. Am. Chem. Soc.* **2017**, *139*, 5085.

[19] Z. Chiguvare, V. Dyakonov, *Phys. Rev. B* **2004**, *70*, 235207.

[20] M. Lenes, M. Morana, C. J. Brabec, P. W. M. Blom, *Adv. Funct. Mater.* **2009**, *19*, 1106.

[21] P. W. M. Blom, V. D. Mihailetchi, L. J. A. Koster, D. E. Markov, *Adv. Mater.* **2007**, *19*, 1551.

[22] L. J. A. Koster, M. Kemerink, M. M. Wienk, K. Maturova, R. A. J. Janssen, *Adv. Mater.* **2011**, *23*, 1670.

[23] S. R. Cowan, A. Roy, A. J. Heeger, *Phys. Rev. B* **2010**, *82*, 245207.

[24] R. Mauer, I. A. Howard, F. Laquai, *J. Phys. Chem. Lett.* **2010**, *1*, 3500.

[25] a) L. Ye, X. C. Jiao, M. Zhou, S. Q. Zhang, H. F. Yao, W. C. Zhao, A. D. Xia, H. Ade, J. H. Hou, *Adv. Mater.* **2015**, *27*, 6046; b) S. Mukherjee, C. M. Proctor, J. R. Tumbleston, G. C. Bazan, T. Q. Nguyen, H. Ade, *Adv. Mater.* **2015**, *27*, 1105.

[26] C. Lee, T. Giridhar, J. Choi, S. Kim, Y. Kim, T. Kim, W. Lee, H. H. Cho, C. Wang, H. Ade, B. J. Kim, *Chem. Mater.* **2017**, *29*, 9407.

[27] K. H. Kim, H. Kang, H. J. Kim, P. S. Kim, S. C. Yoon, B. J. Kim, *Chem. Mater.* **2012**, *24*, 2373.

[28] a) H. Wu, H. J. Fan, S. J. Xu, L. Ye, Y. Guo, Y. P. Yi, H. Ade, X. Z. Zhu, *Small* **2019**, *15*, 1804271; b) L. Ye, H. W. Hu, M. Ghasemi, T. H. Wang, B. A. Collins, J. H. Kim, K. Jiang, J. H. Carpenter, H. Li, Z. K. Li, T. McAfee, J. B. Zhao, X. K. Chen, J. L. Y. Lai, T. X. Ma, J. L. Bredas, H. Yan, H. Ade, *Nat. Mater.* **2018**, *17*, 253.

[29] J. Rivnay, S. C. B. Mannsfeld, C. E. Miller, A. Salleo, M. F. Toney, *Chem. Rev.* **2012**, *112*, 5488.

[30] a) J. Oh, K. Kranthiraja, C. Lee, K. Gunasekar, S. Kim, B. Ma, B. J. Kim, S. H. Jin, *Adv. Mater.* **2016**, *28*, 10016; b) H. Chen, Z. M. Hu, H. Wang, L. Z. Liu, P. J. Chao, J. F.

Qu, W. Chen, A. H. Liu, F. He, *Joule* **2018**, *2*, 1623; c) K. Kranthiraja, S. Kim, C. Lee, K. Gunasekar, V. G. Sree, B. Gautam, K. Gundogdu, S. H. Jin, B. J. Kim, *Adv. Funct. Mater.* **2017**, *27*, 1701256.

[31] J. H. Kim, A. Nizami, Y. Hwangbo, B. Jang, H. J. Lee, C. S. Woo, S. Hyun, T. S. Kim, *Nat. Commun.* **2013**, *4*, 2520.

[32] a) W. Lee, J. H. Kim, T. Kim, S. Kim, C. Lee, J. S. Kim, H. Ahn, T. S. Kim, B. J. Kim, *J. Mater. Chem. A* **2018**, *6*, 4494; b) B. J. Lin, L. Zhang, H. Zhao, X. B. Xu, K. Zhou, S. Zhang, L. Gou, B. B. Fan, L. Zhang, H. P. Yan, X. D. Gu, L. Ying, F. Huang, Y. Cao, W. Ma, *Nano Energy* **2019**, *59*, 277.

[33] J. B. Kim, K. Allen, S. J. Oh, S. Lee, M. F. Toney, Y. S. Kim, C. R. Kagan, C. Nuckolls, Y. L. Loo, *Chem. Mater.* **2010**, *22*, 5762.

[34] Z. H. Wu, C. Sun, S. Dong, X. F. Jiang, S. P. Wu, H. B. Wu, H. L. Yip, F. Huang, Y. Cao, *J. Am. Chem. Soc.* **2016**, *138*, 2004.

A new class of polymer acceptors (P_As, P(BDT2BOY5-X)) consisting of benzodithiophene (BDT) and non-fullerene small molecule accepting units is developed, which shows excellent material compatibility with efficient BDT-based polymer donor (P_D). The resulting all-polymer solar cells show excellent photovoltaic efficiency, thermal stability, and mechanical robustness at the same time, benefitted from high chemical and molecular compatibilities between P_D and P_A.

Efficient, Thermally Stable, and Mechanically Robust All-Polymer Solar Cells Consisting of the Same Benzodithiophene Unit-Based Polymer Acceptor and Donor with High Molecular Compatibility

Jin-Woo Lee,[⊥,†] Cheng Sun,[⊥,§] Boo Soo Ma,[‡] Hyeong Jun Kim,[†] Cheng Wang,[∥] Jong Min Ryu,[/] Chulhee Lim,[†] Taek-Soo Kim,[,‡] Yun-Hi Kim,[*,§] Soon-Ki Kwon,[*,/] and Bumjoon J. Kim[*,†]*